

## ARTICLE OPEN



# Reliability of R2R-printed, flexible electrodes for e-clothing applications

Rafal Sliz<sup>1✉</sup>, Olli-Heikki Huttunen<sup>2</sup>, Elina Jansson<sup>2</sup>, Juhani Kemppainen<sup>3</sup>, Jyrki Schroderus<sup>3</sup>, Marika Kurkinen<sup>2</sup> and Tapio Fabritius<sup>1</sup>

Conformable electrodes are essential for the development of flexible electronics or functional clothing, regardless of their application. Their reliable ability to transfer electric signals or serve as sensing elements in various conditions is vital for the advancement of wearables that will enhance our everyday life. In this research, we concentrate our efforts on the understanding of the influence of elongation and washing on roll-to-roll printed conductive electrodes of various shapes and materials. A large sample set provides data on the breaking mechanisms and how these affect the electrical properties of the electrodes. In addition, the physicochemical analysis offers insights into the electrodes' and materials' behavior in extreme conditions during elongation and washing cycles. The achieved results indicate auspicious nanoparticle shapes and sizes as well as evidence regarding micro-scale breaking mechanisms responsible for electrodes degradation. Utilization of commercially available materials and roll-to-roll printing techniques allow the seamless application of achieved results and the creation of more reliable, flexible electronic devices.

npj Flexible Electronics (2020)4:12; <https://doi.org/10.1038/s41528-020-0076-y>

## INTRODUCTION

In the era of ubiquitous electronics devices, their flexibility and adaptability to our everyday life is becoming critical<sup>1</sup>. Flexible electronics creates a new paradigm where one of the elements of the system is exposed to stress conditions as elongation, bending, or squeezing<sup>2</sup>. Compared to conventional “rigid” electronics, flexible one offers extraordinary applications and new ways of integration strongly supporting the concept of e-clothing and Internet of Things (IoT)<sup>3</sup>.

The concept of flexibility is especially appealing for sensing applications in health and environmental monitoring<sup>4–7</sup>. Health monitoring, where the sensing elements can be placed directly on the skin or implemented into clothing and move together with the measured subject without limiting its maneuverability is one of the ultimate goals supporting the research and development in this field. The ability to embed sensing elements directly into wearables opens a new avenue in the creation of “smart” clothing that monitors the surrounding conditions and informs the owner about abnormalities like illumination, radiation, toxic chemicals, or gases<sup>8–11</sup>. The flexibility is also appealing for energy-harvesting applications<sup>12,13</sup>, allowing the implementation of various energy harvesting methods like indoor and outdoor photovoltaic<sup>13–17</sup>, thermoelectric<sup>18</sup>, or mechanical<sup>19</sup> methods. Another important aspect is the energy storage systems<sup>20,21</sup>, where batteries or supercapacitors, besides being flexible, provide sufficient energy storage to supply the desired portable sub-systems. Also, envisioned advanced wearable systems would need to be equipped with various elements of identification and communication, starting from very simple displays and indicators<sup>22–24</sup>, through identification schemes such as RFID<sup>25,26</sup>, and ending in diverse methods of wireless communication and antenna systems<sup>27</sup>. A truly portable system will consist of several flexible elements interconnected with silicon-based rigid electronic components like processors, memory, and transponders, to name a few. The more flexible the elements, the more independent,

wearable and user-adaptable the system will be, fulfilling the purpose of the e-clothing<sup>28–31</sup>.

Regardless of the implementation, almost all systems require conductive wires either for sensing purposes, to transmit signals, or to deliver electrical energy<sup>32</sup>. Therefore, the role of reliable conductive elements and interconnections is substantial for further development of flexible electronics<sup>33,34</sup>. Electrically conductive lines can be produced by several methods: creating pastes/inks of conductive particles and elastomers that can be further printed or dispersed on the surface of the fabric; depositing carbon or metallic coatings onto fiber surfaces; incorporating hydrophilic comonomers; and by fabricating fibers from aluminum, stainless steel, or other metals<sup>35–38</sup>.

Among the many methods of fabricating conductive components, printing emerges as one of the most promising methods due to the relatively easy implementation, various materials and substrates compatibility, the low cost of fabrication and immense upscaling possibilities thanks to the application of roll-to-roll (R2R) printing techniques<sup>39,40</sup>. Compatibility with various materials is especially important from the perspective of sustainability, where plastic or rare earth elements can be replaced by environmentally friendly materials such as nanocellulose or graphene<sup>41–45</sup>.

A significant amount of research has been conducted to identify, understand, and mitigate the breaking mechanisms responsible for low reliability of printed flexible conductive lines<sup>46–49</sup>. Among many promising concepts and ideas to improve the reliability of the conductive lines, three main strategies have been recognized<sup>50</sup>. The first strategy involves a material composition-oriented approach where carbon or metal nanoparticles/nanowires are mixed with elastomers, providing the desired level of flexibility, often at a price of lower performance due to low conductivity of the elastomers<sup>51</sup>. The second approach includes different structural configurations where the conductive lines are realized in different shapes and structures, providing the ability to elongate without breaking the circuit<sup>52</sup>. The third strategy involves

<sup>1</sup>OPEM Unit, University of Oulu, Erkki Koiso-Kanttilankatu 3, 90570 Oulu, Finland. <sup>2</sup>VTT Technical Research Center of Finland, Kaitoväylä 1, 90570 Oulu, Finland. <sup>3</sup>Polar Electro Oy, Professorintie 5, 90440 Kempele, Finland. ✉email: rafal.sliz@oulu.fi

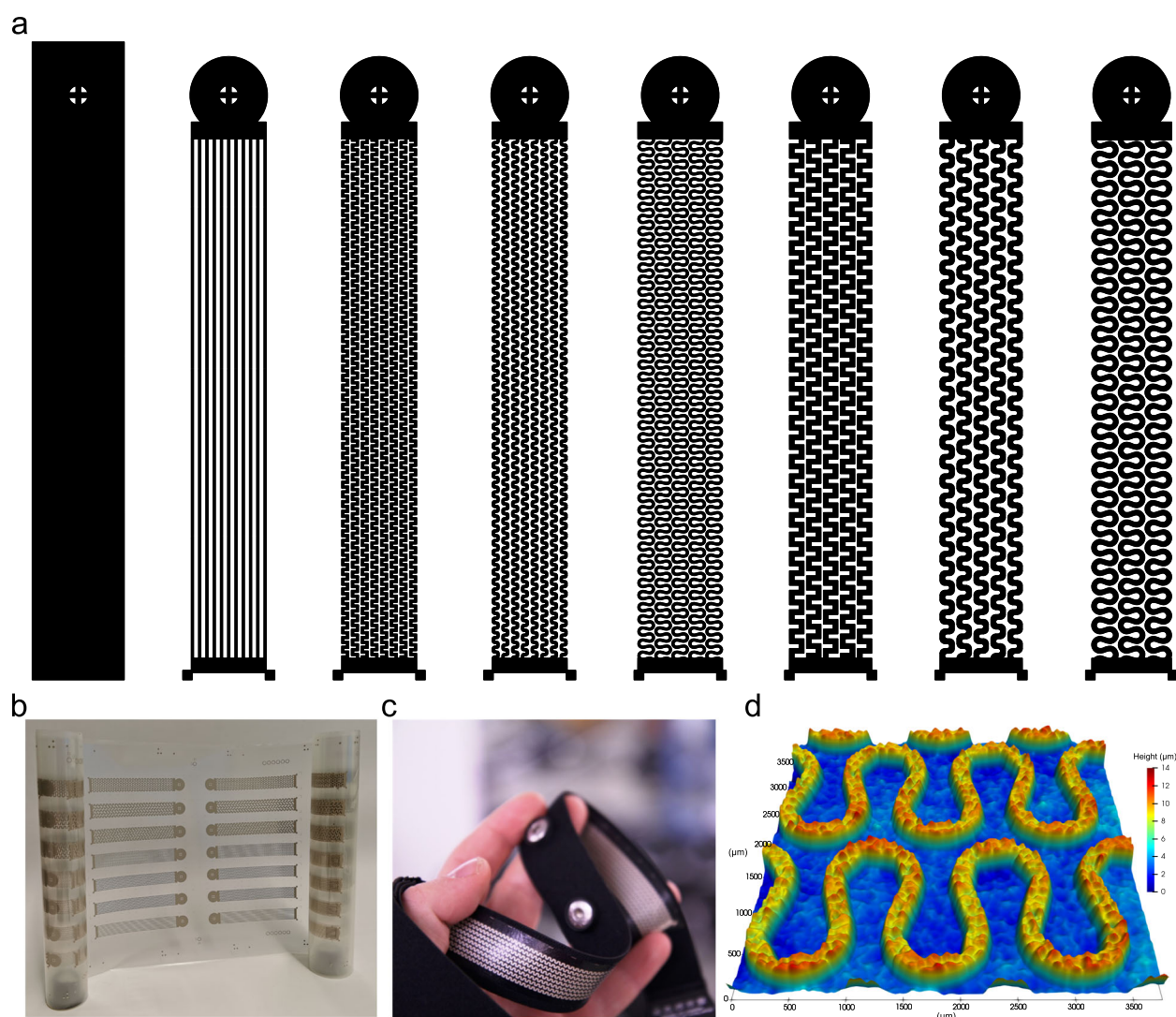


**Fig. 1** Various shape electrodes R2R printed on the flexible substrate (thermoplastic polyurethane). **a** Eight different shaped electrodes (115 × 20 mm). The designed endings allow easy incorporation with the cycling measurement system as well as the integration with the fabric belt for ECG measurements. Panel **b** depicts one of the printing trials where the electrodes were R2R printed on a flexible TPU substrate with a supportive carrier. **c** An exemplary electrode implemented into the stretchable belt used for washing testing and ECG measurements. **d** Profilometric analysis of R2R-printed electrodes.

a concept of protecting the conductive lines with the encapsulation layer, where the conductive lines are embedded in the supportive elastomeric materials<sup>53,54</sup>. Many advancements involve the combination and interconnection of various strategies to achieve the most reliable results<sup>55</sup>.

To ensure full applicability of the fabricated electrodes, besides elongation cycling, we investigated their ability to withstand the washing cycling. This is especially important because washing involves a number of mechanical factors that affect the electrodes such as abrasion, stretching, shearing, bending, flexing, and soaking<sup>56</sup>. In addition, the presence of water and detergents accelerates the degradation process<sup>57</sup>. Although some reports examine the effect of washing on the printed electrodes' behavior, more research is needed to fully understand the impact of the electrode shape and material on the phenomena occurring during washing<sup>58–62</sup>.

In this research, we concentrated our efforts on understanding the influence of elongation and washing on various shaped electrodes, R2R printed on flexible substrates. The variety of the electrode shapes (Fig. 1a) in combination with four different, commercially available conductive pastes R2R printed on flexible

substrates (Fig. 1b) resulted in a testing framework that can be utilized by scientists and engineers in the field of flexible electronics. Importantly, the ultimate goal of this research was to create an outstanding system of conductive electrodes that can be used for precise electrocardiography (ECG) and electroencephalography monitoring (Fig. 1c, Supplementary Fig. S8), where the electrodes can be implemented into clothing and are in direct contact with skin.

During the reliability testing, we utilized the resistance as the main factor indicating the performance of the electrodes (Fig. 2). In addition, we conducted a washing testing where the electrodes were embedded into the fabric and underwent washing procedures, finalized with performance testing. Finally, we performed a physicochemical analysis of the printed electrodes to understand the breaking mechanism and significance of both elongation and washing on the performance of the electrodes.

## RESULTS

Resistance is one of the most typical indicators of the quality of the electrodes, and, therefore, it was used to estimate the

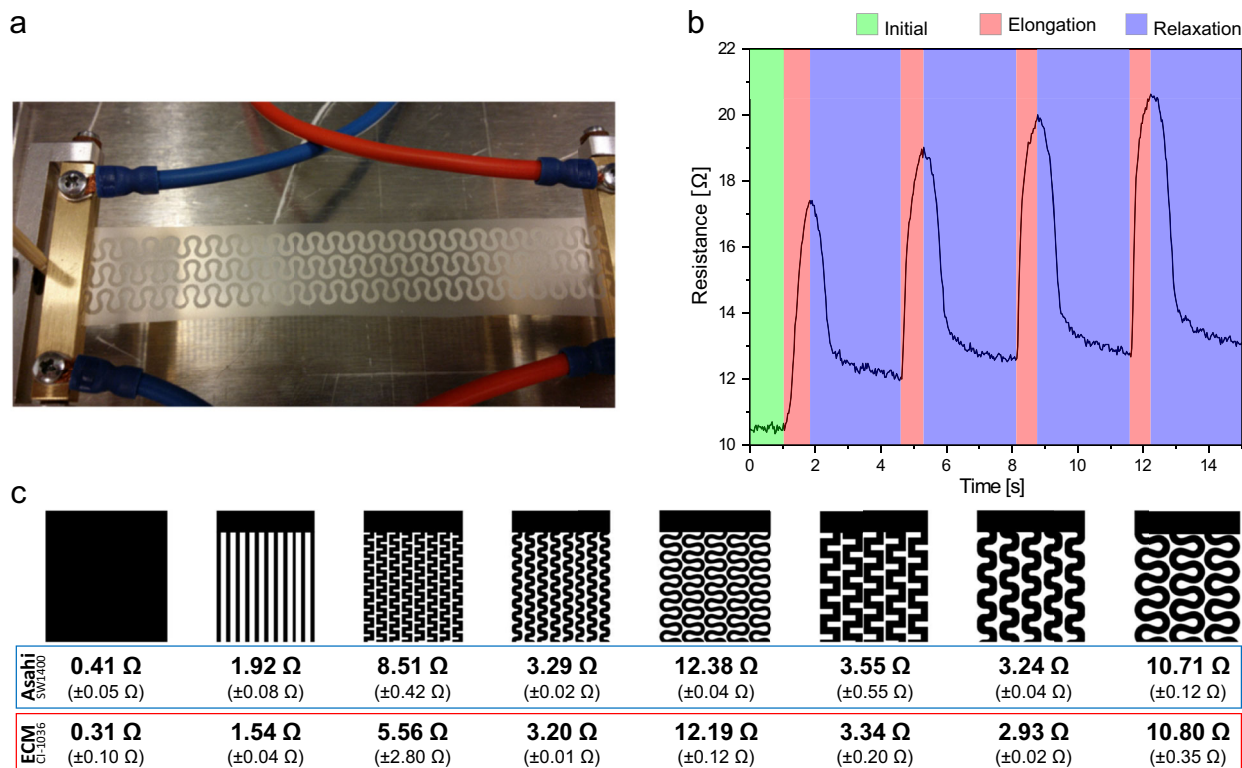


**Fig. 2 Resistance measurements.** **a** Four-probe resistance vs. elongation measurement system with 30 Hz sampling rate. **b** An exemplary plot of the electrode resistance variation during the elongation cycling. **c** The initial resistance of the various shaped electrodes for Asahi SW1400 and ECM CI-1036 screen-printing pastes.

electrode performance during the reliability cycling (see Fig. 2a and the elongation video in the Supplementary Information). The initial tests provided data on how the resistance changes during a single elongation cycle (Fig. 2b) as well as during an extended amount of time. As seen in Fig. 2b, the single elongation cycle can be divided into two main phases: elongation and relaxation. During elongation, the electrode is under stress and the resistance increases. During relaxation, the electrode comes back to its initial length; however, the resistance increases insignificantly with every cycle. This behavior has been recognized and elaborated on by Liang et al.<sup>63</sup>.

Before starting the elongation cycling, we measured the initial resistance of the electrodes printed with Asahi SW1400 and ECM CI-1036 pastes (Fig. 2c) as well as their thicknesses, which were  $10.4 \pm 0.8$  and  $8.6 \pm 0.25$  μm for Asahi SW1400 and ECM CI-1036, respectively. The tests provided a set of data for various pastes (Asahi SW1400, ECM CI-1036, ECM CI-4040, PPG XCMB-590) and shapes (Fig. 1a). After completing the measurements, we selected the most promising two pastes for further testing and analysis (Asahi SW1400 and ECM CI-1036). Importantly, the results for the remaining pastes and tests of additional annealing treatment are available in the Supplementary Information document. ECM CI-4040 and PPG XCMB-590 pastes were excluded from the main manuscript file due to their poor performance during this study and to ensure the clarity of this document. As evaluation criteria for excluding some of the pastes, we utilized the increase of the resistance during the elongation cycles. The material was considered as well-performing if at least 50% of the measured samples survived the elongation cycling without exceeding the resistance of 10 kΩ. Figure 3 depicts the resistance change of the flexible electrodes of eight different shapes printed with two of the most promising materials.

Regardless of the shape, after 10,000 (10% elongation) cycles, the ECM CI-1036 paste demonstrated more stable behavior in

both instances: during elongation and relaxation periods. Also, the resistance of the electrodes printed with ECM CI-1036 was lower than Asahi SW1400, both at the beginning and throughout the cycling. In terms of the influence of the pattern size of the electrode on its reliability, the large shapes exhibited better endurance. Furthermore, for the large shapes, the difference between the resistance during elongation and relaxation was the lowest. For the full coverage electrodes, the resistance remains low in both cases. However, for Asahi SW1400, after approximately 17,000 cycles, the resistance during elongation starts to peak notably, indicating the beginning of the breakage. In terms of the impact of the pattern shape on the electrode performance, we did not find considerable differences.

To better understand the reasons for the increased resistance and breaking mechanism of the electrodes, we performed a scanning electron microscopy (SEM) analysis of the electrode surfaces and compared the results to the untreated ones (Fig. 4). Regardless of the SEM magnification, the best two pastes do not reveal any significant changes on the surface of the electrodes. Importantly, larger-scale images (×40) illustrate that the surface of the electrodes remains smooth and cracks-free after the elongation process. At the same time, the remaining poor-performing pastes depicted in Supplementary Fig. S5 show small dents and cracks that could be attributed to their poor performance. SEM images also disclose the size of the Ag particles/flakes that the pastes are composed of—Asahi SW1400 ~4 μm and ECM CI-1036 ~7 μm.

To understand better the influence of the pattern size on electrode behavior, we compared the SEM images of the elongated electrodes after the full elongation cycle. To highlight the differences, the electrodes were elongated by 5% and the images acquired (details in the Methods section). SEM images (Fig. 5, Supplementary Fig. S6 and S7) reveal that, compared to the small patterns, the large ones are more resilient to cracks and voids' formation during elongation cycling, regardless of the paste used.

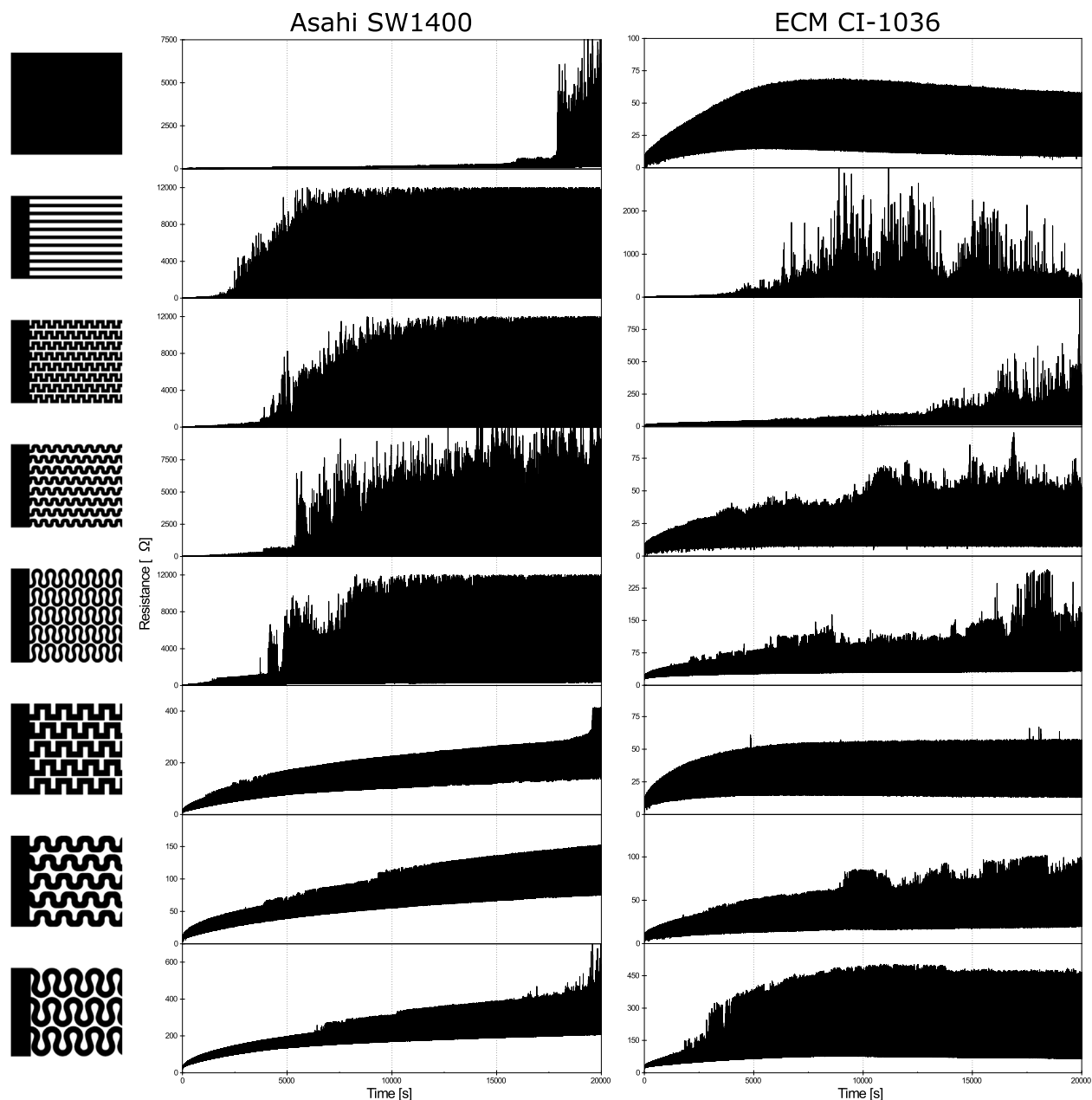


**Fig. 3** The resistance of various shaped electrodes for two best-performing pastes. The plots depict the change of resistance during the elongation and relaxation cycle. The full cycle consisted of 10,000, 10% elongation cycles, at speed 0.5 Hz. The resistance axis scale varies, and it is adapted to each resistance range to illustrate the behavior of the electrodes better. The plots for the remaining pastes (ECM CI-4040 and XCMB-590) are available in the Supplementary Information.

Supplementary Figures S6 and S7 show that the cracks in the small pattern electrodes range from 4 to 5  $\mu\text{m}$ , while, in the large pattern electrodes, the cracks are from 1 to 2  $\mu\text{m}$ , at the same level of elongation. Regarding the impact of the pattern shape on electrode performance, as in the resistance measurements, the SEMs images do not indicate significant differences.

Consequently, we attached the fresh set of printed-on TPU electrodes to a stretchable belt as in Fig. 1c and conducted washing cycles. After washing, we performed the physicochemical analysis of the electrodes with an SEM microscope. As seen in Fig. 6, regardless of the electrode material, the images point out the existence of cracks within the electrode structure, as opposed to the unwashed samples where the cracks are not present. Higher magnification images reveal more information about the density and size of the cracks.

After imaging, we utilized the SEM microscope, equipped with EDS functionality to analyze the chemical composition of the electrodes before and after washing. The results of the SEM-EDS analysis are presented in Table 1. The elemental analysis discloses an insignificant change in the amount of oxygen and chlorine and a more recognizable decrease in the amount of silver and an increase of carbon in the washed belts, for both pastes. However, the elemental composition changes are more notable for ECM CI-1036.

In addition, we analyzed the impact of the washing on the surface roughness ( $R_a$ —arithmetic average and  $R_q$ —root mean squared) of the electrodes. The results presented in Table 2 show that washing increases the roughness of the surface by approximately 38% and 170% for Asahi SW1400 and ECM CI-1036, respectively.

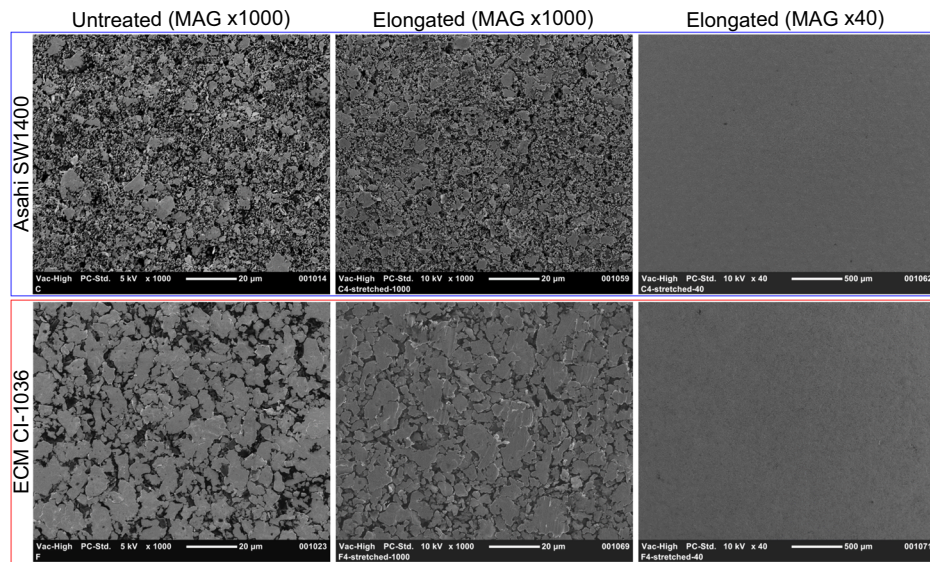


**Fig. 4** SEM images of the two best-performing pastes before and after the elongation cycles—full coverage electrodes. The figures illustrate no substantial changes on the surface of the electrodes before and after the cycling. The large area figures (MAG  $\times 40$ ) demonstrate a smooth surface, free from cracks or dents, regardless of the paste used.

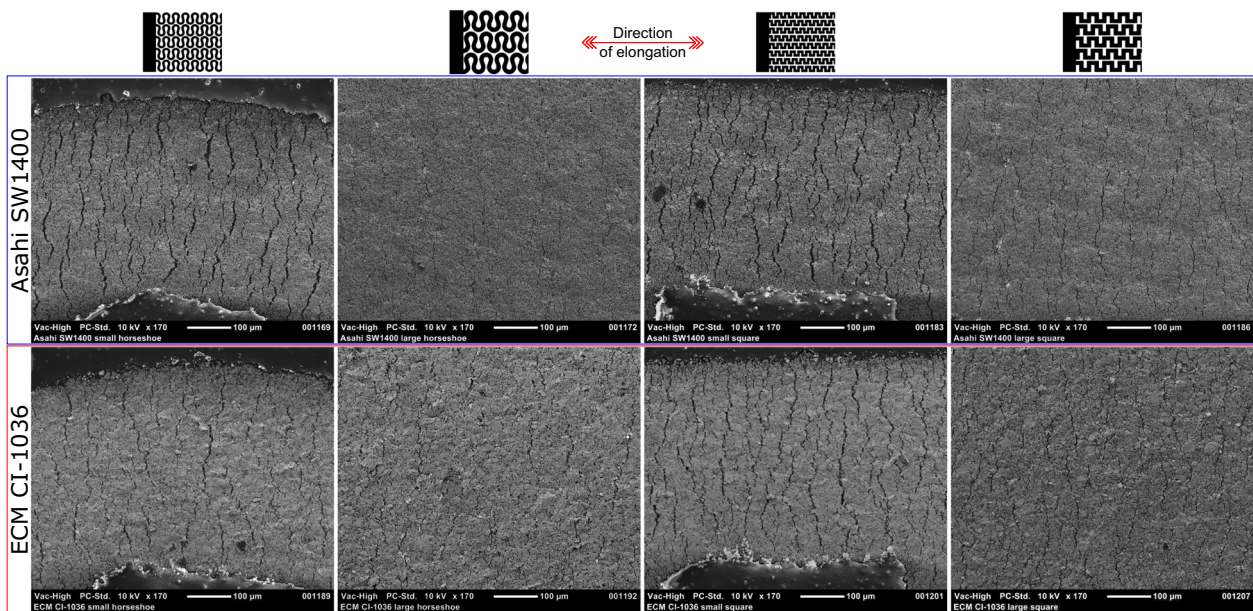


**Fig. 5** SEM analysis of the influence of elongation on electrodes of various size patterns for Asahi SW1400 and ECM CI-1036 pastes. SEM images at  $\times 170$  magnification show a large number of wide cracks for small patterns. Although the larger patterns also show the presence of cracks, their size is notably smaller. This behavior occurs regardless of the paste used. Broadened SEM analysis for large and small patterns at various magnifications is available in the Supplementary Information document (Supplementary Fig. S6 and S7).

Finally, we measured the resistance of the electrodes after the washing cycle. The results in Table 3 illustrate the difference between unwashed and washed belts—after washing, the resistance of the full coverage electrodes increases approximately 520 and 1100 times for Asahi SW1400 and ECM CI-1036, respectively. At the same time, the horseshoe electrodes lose their conductive properties, regardless of the paste used.

## DISCUSSION

The ultimate goal of this work was to test various shapes and pastes and create a framework that can be utilized for printed and flexible systems measuring human vital signs. Therefore, the

electrode surface was not protected by any encapsulation. The reliability cycling that used the resistance as the primary indicator pointed out a few important aspects related to the pattern size of the electrode and the material used for printing. The data indicate that Asahi SW1400 and EMC CI-1036 significantly overperformed the remaining pastes in terms of the resistance and the reliability during elongation and washing cycles. After physicochemical analysis, we realized that one of the main reasons for such behavior might have been the size of the conductive particles/flakes used in the paste formulation. Asahi SW1400 and ECM CI-1036 are composed of Ag particles of a size of  $\sim 4$  and  $\sim 7$   $\mu\text{m}$ , respectively, while PPG XCMB-590 and ECM CI-4040 consist of particles of a size above 10  $\mu\text{m}$ . Although larger conductive

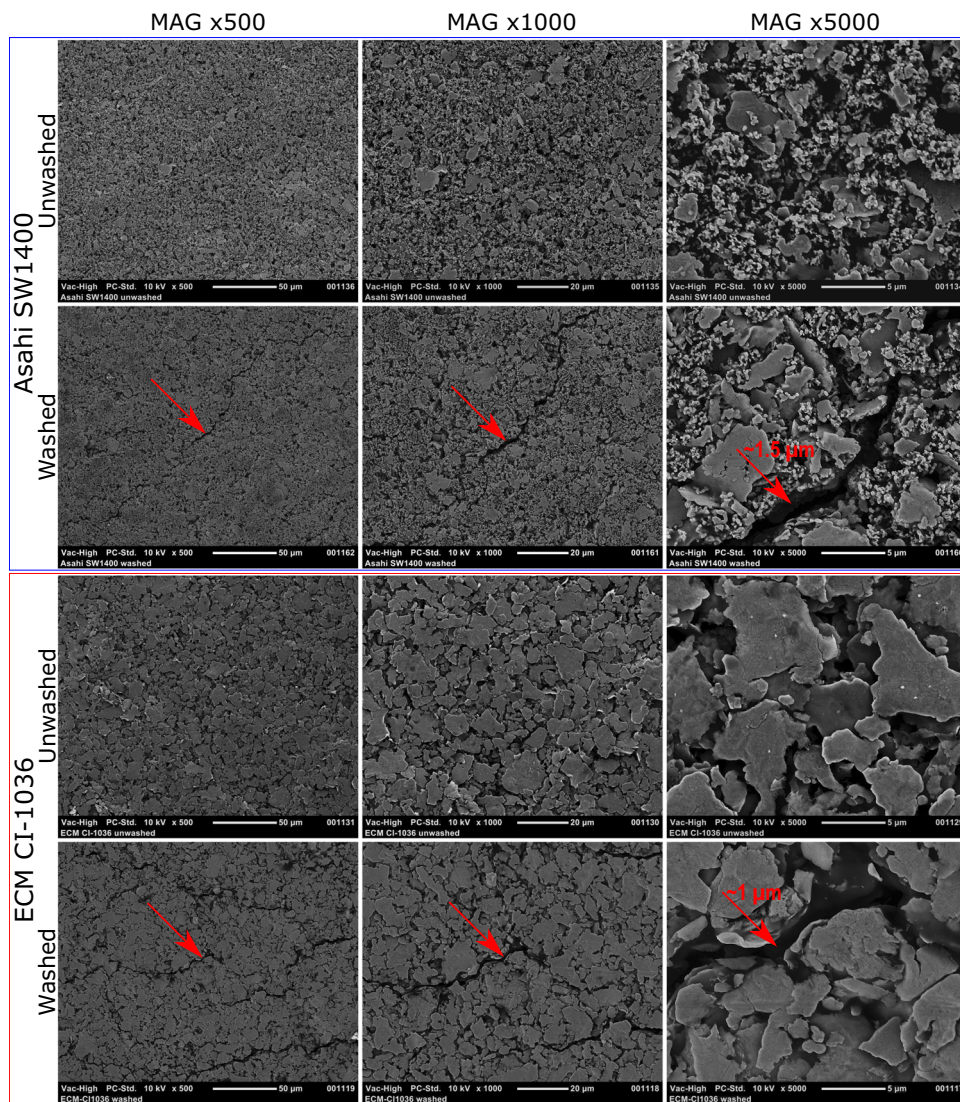


**Fig. 6** Macroscopic comparison of washed and unwashed electrodes (Asahi SW1400 and ECM CI-1036) at various magnifications. SEM images at  $\times 500$  magnification show the existence of cracks on the surface of the washed samples while the unwashed samples remain intact. SEM image at  $\times 1000$  magnification points out the presence of cracks over the surface of the washed samples. The SEM images at magnification  $\times 5000$  show the details of the cracks that are approximately 1–2  $\mu\text{m}$  wide. Red arrows emphasize the location of the cracks at various SEM magnifications.

particles keep the resistance of the electrodes lower, they are more prone to flake off and/or create larger voids due to elongation cycling and washing. Smaller particles used in Asahi SW1400 and ECM CI-1036 provide better mechanical properties at the price of lower conductivity, especially during elongation.

The analysis of the influence of the pattern size on the electrodes' performance suggests that the large patterns withstand the elongation process better and provide better conductive properties. Figure 5 and Supplementary Figs. S6, and S7 show a similar number of cracks for both sizes of the patterns. However, the cracks and voids in the small patterns are approximately 2–3 times larger. The main differences between the large and small patterns are the radius and the width of the conductive lines. These two factors have been recognized as important aspects affecting the performance of the electrodes<sup>64,65</sup>. Even the cracks' distribution on the surface of the electrodes implies an equal distribution of the strain along the elongation axis, pointing at the width of the conductive lines as the main reason for their different behavior. In essence, the wider

lines, in the larger patterns, are more resistant to mechanical stress. Also, the wider lines reduce the probability that the conductive path in the electrode line is damaged permanently by the increasing amount of cracks. Importantly, although the full coverage electrodes showed the best performance regardless of the paste, the elongation video in the Supplementary Information demonstrates a tremendous number of cracks occurring during the elongation process. Noteworthy, the resistance and SEM results imply that the pattern shape (within the same pattern size) affects the resistance of the electrodes but is not critical for the stable operation of the electrodes.

Additional annealing performed on Asahi SW1400 paste indicates that additional heat treatment is not beneficial and increases the degradation of the printed electrodes, represented by resistance spikes after 10,000 s of an elongation cycle (Supplementary Fig. S4). When compared, the single annealed electrodes show more stable performance throughout the cycling process. The exact reasons for such behavior need further investigation.

**Table 1.** SEM-EDS elemental analysis of the surface of washed and unwashed electrodes.

Element	Asahi SW1400		ECM CI-1036	
	Unwashed belt [%]	Washed belt [%]	Unwashed belt [%]	Washed belt [%]
C	5.03 ± 0.22	6.69 ± 0.44	2.04 ± 0.61	6.79 ± 0.12
O	7.10 ± 0.15	7.54 ± 0.06	4.34 ± 0.55	4.33 ± 0.16
Cl	0.29 ± 0.10	0.02 ± 0.03	2.01 ± 0.28	2.18 ± 0.10
Ag	87.58 ± 0.08	85.48 ± 0.43	91.61 ± 0.87	86.70 ± 0.22

**Table 2.** Surface roughness comparison of washed and unwashed belts.

Surface roughness	Asahi SW1400		ECM CI-1036	
	Unwashed belt [μm]	Washed belt [μm]	Unwashed belt [μm]	Washed belt [μm]
$R_a$	1.38 ± 0.06	1.90 ± 0.27	0.51 ± 0.03	1.39 ± 0.09
$R_q$	1.72 ± 0.08	2.40 ± 0.30	0.69 ± 0.03	1.77 ± 0.02

The applied washing tests reveal how critical the aspect of water and detergent are during mechanical stress. The SEM results point out that water washes away the material from the voids caused by mechanical stress. At the same time, the SEM-EDS results specify that the amount of silver on the surface decreases while carbon content is increasing, indicating that silver particles, especially the larger ones, are more prone to washing. The roughness analysis shows that washing introduces substantial mechanical stresses to the electrodes, and water and detergents wash away any particles that are not fully immobilized, leading to rough surfaces and cracks that increase resistance and contribute to the breaking of the electrodes. The results presented in Table 3 point out that washing is destructive for electrodes, regardless of the shape and only a full coverage electrode withstood the washing process, maintaining the conductive properties. Although the full coverage electrodes remained conductive, their resistances were unacceptably high.

Finally, the applicability of the printed electrodes for heart rate measurements was successfully verified—the electrodes presented outstanding data acquisition of the ECG signal from the skin of the object under test (Supplementary Fig. S8).

To conclude, this work provides information regarding the behavior of R2R-printed flexible electrodes exposed to stress conditions during elongation and washing. The achieved results indicate that pastes consisting of conductive particles of a size below ~8 μm allow the fabrication of flexible and reliable electrodes. It is noteworthy that the utilization of smaller conductive particles might compromise the high conductivity of the electrodes, which might be undesirable for some applications. In addition, the results reveal the reasons why the large-size patterns in the electrodes have better electrical properties, compared to the small ones, regardless of the paste material. Finally, the results also point out the need for more research related to washing of the flexible electronic components as this seems to be especially destructive.

## METHODS

Platilon UO73 thermoplastic polyurethane was selected as the most suitable base substrate. However, due to its stretchability, it required an

**Table 3.** The resistance of the different shape electrodes (full coverage and horseshoe) after the washing cycle.

	Full coverage		Horseshoe	
	Unwashed	Washed	Unwashed	Washed
Asahi SW1400	0.41 ± 0.05 Ω	212 ± 15.5 Ω	10.71 ± 0.12 Ω	—
ECM CI-1036	0.31 ± 0.10 Ω	344 ± 42.4 Ω	10.80 ± 0.35 Ω	—

inelastic carrier film serving as a carrier in the R2R process due to substantial web tension. Based on the experimental results (Supplementary Fig. S1) and vendor information, the pastes applied in this research required annealing at temperatures of 120 °C or higher, making the PE carrier (Platilon UO73) R2R incompatible. Therefore, prior to the printing, the PE carrier was replaced with an inelastic and more thermally stable PET. The electrodes of various patterns (Fig. 1a) were fabricated using rotary screen printing. Printing was carried out using silver pastes (Asahi SW1400, ECM CI-1036, ECM CI-4040 and PPG XCMB-590) and a rotary screen (Stork steel mesh 305 in.<sup>−1</sup>) with a speed of 2 m/min (Supplementary Fig. S9). Then, hot air curing was carried out in a convection air oven with an air temperature of 120 °C for 2 min, followed by a sequential 2 min in 120 °C three times to ensure curing. For the double annealing test, the heat treatment cycle was repeated.

The elongation was performed using the four-probe resistance measurement system (Fig. 2a), introducing 10,000 elongation cycles of 10% at a frequency of 0.5 Hz. The system was composed of an Agilent 34401A digital multimeter connected to the computer with LabView software for the data acquisition. The resistance of the electrode was measured with a frequency of 30 Hz. The same system was used to measure the initial resistance of the electrodes.

During the washing procedure, untreated electrodes on the TPU substrate were attached to stretchable fabric belts (Fig. 1c), placed in the washing bag, and inserted into a Siemens WD14H540DN washing machine (Supplementary Fig. S10a). According to the producer, the energy consumption when the device is connected is approximately 2,200 W. Approximately 10 ml of washing powder—Ariel A+ (Supplementary Fig. S10b) was added to the detergent compartment drawer. No bleaching detergent was used. The Mixed Fabrics program, without additional functions, was used for the washing cycle. The program is designated for “textiles made of cotton and easy-care textiles, different types of textiles which can be washed together”. The temperature and the spinning were set to 40 °C and 1000 r.p.m., respectively. The washing cycle lasted for approximately 63 min. The washing was followed by the drying process on a clothes drying rack, at room temperature. The washing and drying cycles were repeated 10 times. The raw stretchable fabric belts exhibited ~50% elongation when 10 N force was applied. In terms of mechanical performance, the belts showed no degradation signs after 30,000 cycles at 30% elongation (×3 cycling and ×3 elongation compared to the electrodes).

SEM images were acquired using an SEM NeoScope JCM-5000 at various magnifications as indicated in the respective figures. To emphasize the difference in the behavior of various size patterns in the SEM images (Fig. 5, Supplementary Fig. S6 and S7), the electrodes were elongated by 5% and attached to a double-sided carbon tape that kept the electrode elongation during the SEM imaging. The EDS measurements of the area of 0.05 mm<sup>2</sup> were performed with Zeiss ULTRA plus FESEM, equipped with an EDS detector for elemental analysis of the surface. The roughness measurements of the area of 0.3 mm<sup>2</sup>, as well as profile extraction, were conducted using a Bruker ContourGT optical profilometer in VSI mode.

## DATA AVAILABILITY

The data that support the findings of this study are available in the supplementary document or from the authors.

Received: 19 February 2020; Accepted: 29 May 2020;  
Published online: 01 July 2020

## REFERENCES

- Nathan, A. et al. Flexible electronics: the next ubiquitous platform. *Proc. IEEE* **100**, 1486–1517 (2012).
- Wong, W. S. & Salleo, A. *Flexible Electronics, Materials and Applications* (Springer, 2009).
- Zhan, Y., Mei, Y. & Zheng, L. Materials capability and device performance in flexible electronics for the Internet of Things. *J. Mater. Chem. C* **2**, 1220–1232 (2014).
- Wang, X., Liu, Z. & Zhang, T. Flexible sensing electronics for wearable/attachable health monitoring. *Small* **13**, 1–19 (2017).
- Liu, Y., Pharr, M. & Salvatore, G. A. Lab-on-Skin: a review of flexible and stretchable electronics for wearable health monitoring. *ACS Nano* **11**, 9614–9635 (2017).
- Schwartz, G. et al. Flexible polymer transistors with high pressure sensitivity for application in electronic skin and health monitoring. *Nat. Commun.* **4**, 1859–1867 (2013).
- Trung, T. Q. & Lee, N. E. Flexible and stretchable physical sensor integrated platforms for wearable human-activity monitoring and personal healthcare. *Adv. Mater.* **28**, 4338–4372 (2016).
- Singh, E., Meyyappan, M. & Nalwa, H. S. Flexible graphene-based wearable gas and chemical sensors. *ACS Appl. Mater. Interfaces* **9**, 34544–34586 (2017).
- Kukkola, J. et al. Novel printed nanostructured gas sensors. *Procedia Eng.* **25**, 896–899 (2011).
- Sliz, R. et al. Stable colloidal quantum dot inks enable inkjet-printed high-sensitivity infrared photodetectors. *ACS Nano* **13**, 11988–11995 (2019).
- Khan, S., Lorenzelli, L. & Dahiya, R. S. Technologies for printing sensors and electronics over large flexible substrates: a review. *IEEE Sens. J.* **15**, 3164–3185 (2015).
- Yang, Y. et al. Flexible hybrid energy cell for simultaneously harvesting thermal, mechanical, and solar energies. *ACS Nano* **7**, 785–790 (2013).
- Wu, H., Huang, Y. A., Xu, F., Duan, Y. & Yin, Z. Energy harvesters for wearable and stretchable electronics: from flexibility to stretchability. *Adv. Mater.* **28**, 9881–9919 (2016).
- Kim, B. J. et al. Highly efficient and bending durable perovskite solar cells: toward a wearable power source. *Energy Environ. Sci.* **8**, 916–921 (2015).
- Sliz, R., Suzuki, Y., Fabritius, T. & Myllylä, R. Influence of temperature on wetting properties of thin films in organic solar cells applications. *Colloids Surf. A Physicochem. Eng. Asp.* **443**, 182–187 (2014).
- Ylikunnari, M. et al. Flexible OPV modules for highly efficient indoor applications. *Flex. Print. Electron.* **5**, 14008–14020 (2020).
- Shaheen, S. E., Radspinner, R., Peyghambarian, N. & Jabbour, G. E. Fabrication of bulk heterojunction plastic solar cells by screen printing. *Appl. Phys. Lett.* **79**, 2996–2998 (2001).
- Kim, S. J., We, J. H. & Cho, B. J. A wearable thermoelectric generator fabricated on a glass fabric. *Energy Environ. Sci.* **7**, 1959–1965 (2014).
- Lin, L. et al. Transparent flexible nanogenerator as self-powered sensor for transportation monitoring. *Nano Energy* **2**, 75–81 (2013).
- Peng, H. J., Huang, J. Q. & Zhang, Q. A review of flexible lithium-sulfur and analogous alkali metal-chalcogen rechargeable batteries. *Chem. Soc. Rev.* **46**, 5237–5288 (2017).
- Gaikwad, A. M., Arias, A. C. & Steingart, D. A. Recent progress on printed flexible batteries: mechanical challenges, printing technologies, and future prospects. *Energy Technol.* **3**, 305–328 (2014).
- Choi, S. et al. Highly flexible and efficient fabric-based organic light-emitting devices for clothing-shaped wearable displays. *Sci. Rep.* **7**, 1–8 (2017).
- Jokinen, K. et al. Luminescence and spectrum variations caused by thermal annealing in undoped and doped polyfluorene OLEDs. *Solid. State Electron.* **103**, 184–189 (2015).
- Pardo, D. A., Jabbour, G. E. & Peyghambarian, N. Application of screen printing in the fabrication of organic light-emitting devices. *Adv. Mater.* **12**, 1249–1252 (2000).
- Abad, E. et al. Flexible tag microlab development: gas sensors integration in RFID flexible tags for food logistic. *Sens. Actuators B Chem.* **127**, 2–7 (2007).
- Leng, T. et al. Graphene nanoflakes printed flexible meandered-line dipole antenna on paper substrate for low-cost RFID and sensing applications. *IEEE Antennas Wirel. Propag. Lett.* **15**, 1565–1568 (2016).
- Xie, Z., Avila, R., Huang, Y. & Rogers, J. A. Flexible and stretchable antennas for biointegrated electronics. *Adv. Mater.* **1902767**, 1–16 (2019).
- Fan, F. R., Tang, W. & Wang, Z. L. Flexible nanogenerators for energy harvesting and self-powered electronics. *Adv. Mater.* **28**, 4283–4305 (2016).
- Jeong, C. K. et al. Self-powered fully-flexible light-emitting system enabled by flexible energy harvester. *Energy Environ. Sci.* **7**, 4035–4043 (2014).
- Park, S. et al. Self-powered ultra-flexible electronics via nano-grating-patterned organic photovoltaics. *Nature* **561**, 516–521 (2018).
- Kim, J. et al. Miniaturized flexible electronic systems with wireless power and near-field communication capabilities. *Adv. Funct. Mater.* **25**, 4761–4767 (2015).
- Matsuhisa, N. et al. Printable elastic conductors with a high conductivity for electronic textile applications. *Nat. Commun.* **6**, 7461–7672 (2015).
- Perelaer, J. et al. Printed electronics: the challenges involved in printing devices, interconnects, and contacts based on inorganic materials. *J. Mater. Chem.* **20**, 8446–8453 (2010).
- Vosgueritchian, M., Lipomi, D. J. & Bao, Z. Highly conductive and transparent PEDOT:PSS films with a fluorosurfactant for stretchable and flexible transparent electrodes. *Adv. Funct. Mater.* **22**, 421–428 (2012).
- Schindler, W. D. & Hauser, P. J. *Chemical Finishing of Textiles* (Woodhead Publishing, 2004).
- Rattfält, L., Lindén, M., Hult, P., Berglin, L. & Ask, P. Electrical characteristics of conductive yarns and textile electrodes for medical applications. *Med. Biol. Eng. Comput.* **45**, 1251–1257 (2007).
- Pudas, M., Halonen, N., Granat, P. & Vähäkangas, J. Gravure printing of conductive particulate polymer inks on flexible substrates. *Prog. Org. Coat.* **54**, 310–316 (2005).
- Kamyshny, A. & Magdassi, S. Conductive nanomaterials for printed electronics. *Small* **10**, 3515–3535 (2014).
- Huttunen, O. H. et al. Roll-to-roll screen-printed silver conductors on a polydimethyl siloxane substrate for stretchable electronics. *Ind. Eng. Chem. Res.* **58**, 19909–19916 (2019).
- Choi, H. W., Zhou, T., Singh, M. & Jabbour, G. E. Recent developments and directions in printed nanomaterials. *Nanoscale* **7**, 3338–3355 (2015).
- Hoeng, F., Denneulin, A. & Bras, J. Use of nanocellulose in printed electronics: a review. *Nanoscale* **8**, 13131–13154 (2016).
- Jung, Y. H. et al. High-performance green flexible electronics based on biodegradable cellulose nanofibril paper. *Nat. Commun.* **6**, 7170–7181 (2015).
- Hyun, W. J., Secor, E. B., Hersam, M. C., Frisbie, C. D. & Francis, L. F. High-resolution patterning of graphene by screen printing with a silicon stencil for highly flexible printed electronics. *Adv. Mater.* **27**, 109–115 (2015).
- Jinno, H. et al. Stretchable and waterproof elastomer-coated organic photovoltaics for washable electronic textile applications. *Nat. Energy* **2**, 780–785 (2017).
- Hartmann, R. et al. Interactions between aminated cellulose nanocrystals and quartz: adsorption and wettability studies. *Colloids Surf. A Physicochem. Eng. Asp.* **489**, 207–215 (2016).
- Baca, A. J. et al. Semiconductor wires and ribbons for high-performance flexible electronics. *Angew. Chem. Int. Ed.* **47**, 5524–5542 (2008).
- Rogers, J. A., Someya, T. & Huang, Y. Materials and mechanics for stretchable electronics. *Science* **327**, 1603–1607 (2010).
- Ma, Y., Feng, X., Rogers, J. A., Huang, Y. & Zhang, Y. Design and application of 'J-shaped' stress-strain behavior in stretchable electronics: a review. *Lab Chip* **17**, 1689–1704 (2017).
- Happonen, T., Ritvonen, T., Korhonen, P., Häkkinen, J. & Fabritius, T. Bending reliability of printed conductors deposited on plastic foil with various silver pastes. *Int. J. Adv. Manuf. Technol.* **82**, 1663–1673 (2016).
- Kim, D. H. & Rogers, J. A. Stretchable electronics: materials strategies and devices. *Adv. Mater.* **20**, 4887–4892 (2008).
- Lee, Y. I., Kim, S., Jung, S. B., Myung, N. V. & Choa, Y. H. Enhanced electrical and mechanical properties of silver nanoplatelet-based conductive features direct printed on a flexible substrate. *ACS Appl. Mater. Interfaces* **5**, 5908–5913 (2013).
- Fan, J. A. et al. Fractal design concepts for stretchable electronics. *Nat. Commun.* **5**, 1–8 (2014).
- Li, K. et al. A generic soft encapsulation strategy for stretchable electronics. *Adv. Funct. Mater.* **29**, 1–12 (2019).
- Bossuyt, F., Vervust, T. & Vanfleteren, J. Stretchable electronics technology for large area applications: fabrication and mechanical characterization. *IEEE Trans. Compon. Packag. Manuf. Technol.* **3**, 229–235 (2013).
- Harris, K. D., Elias, A. L. & Chung, H. J. Flexible electronics under strain: a review of mechanical characterization and durability enhancement strategies. *J. Mater. Sci.* **51**, 2771–2805 (2016).
- Zaman, S. U., Tao, X., Cochrane, C. & Koncar, V. Market readiness of smart textile structures—reliability and washability. *IOP Conf. Ser. Mater. Sci. Eng.* **459**, 12071–12077 (2018).

57. Ismar, E., Zaman, Suz, Tao, X., Cochrane, C. & Koncar, V. Effect of water and chemical stresses on the silver coated polyamide yarns. *Fibers Polym.* **20**, 2604–2610 (2019).
58. Achilli, A., Pani, D. & Bonfiglio, A. Characterization of screen-printed textile electrodes based on conductive polymer for ECG acquisition. *Comput. Cardiol.* (2010) **44**, 1–4 (2017).
59. Hsu, P. C. et al. A printed physiological monitoring module in e-textile. *2018 Int. Flex. Electron. Technol. Conf. IFETC 2018*, Ottawa, ON, Canada, 1–2 (2018).
60. Achilli, A., Bonfiglio, A. & Pani, D. Design and characterization of screen-printed textile electrodes for ECG monitoring. *IEEE Sens. J.* **18**, 4097–4107 (2018).
61. Preston, D. J. et al. Heat transfer enhancement during water and hydrocarbon condensation on lubricant infused surfaces. *Sci. Rep.* **8**, 1–9 (2018).
62. Kye, M. J. et al. “Drop-on-textile” patternable aqueous PEDOT composite ink providing highly stretchable and wash-resistant electrodes for electronic textiles. *Dye. Pigm.* **155**, 150–158 (2018).
63. Liang, J. et al. Silver nanowire percolation network soldered with graphene oxide at room temperature and its application for fully stretchable polymer light-emitting diodes. *ACS Nano* **8**, 1590–1600 (2014).
64. Hocheng, H. & Chen, C. M. Design, fabrication and failure analysis of stretchable electrical routings. *Sensors* **14**, 11855–11877 (2014).
65. Marchiori, B., Delattre, R., Hannah, S., Blayac, S. & Ramuz, M. Laser-patterned metallic interconnections for all stretchable organic electrochemical transistors. *Sci. Rep.* **8**, 1–9 (2018).

## ACKNOWLEDGEMENTS

This research was supported by the postdoctoral research fellow grant of the Academy of Finland (grant no. 296890). The authors also express their gratitude for the financial support received from the Academy of Finland's FIRI funding (grant no. 320017 and 320020) and Tekes Grant (Hilla) no. 3896/31/2014. Pekka Ontero and Mikko Hietala are acknowledged for roll-to-roll printing machine operation. Finally, the authors acknowledge Jakub Czajkowski for his invaluable contribution to this project in terms of layout and measurement system development.

## AUTHOR CONTRIBUTIONS

R.S. conceived the ideas and designed the project, performed characterization and data analysis, and wrote the article with contribution from the remaining authors. O.-H.H. and E.J. developed and supervised the printing trials. J.K. was involved in the

washing trials. T.F. and M.K. supported the project and commented on the manuscript.

## COMPETING INTERESTS

The authors declare no competing interests.

## ADDITIONAL INFORMATION

**Supplementary information** is available for this paper at <https://doi.org/10.1038/s41528-020-0076-y>.

**Correspondence** and requests for materials should be addressed to R.S.

**Reprints and permission information** is available at <http://www.nature.com/reprints>

**Publisher's note** Springer Nature remains neutral with regard to jurisdictional claims in published maps and institutional affiliations.



**Open Access** This article is licensed under a Creative Commons Attribution 4.0 International License, which permits use, sharing, adaptation, distribution and reproduction in any medium or format, as long as you give appropriate credit to the original author(s) and the source, provide a link to the Creative Commons license, and indicate if changes were made. The images or other third party material in this article are included in the article's Creative Commons license, unless indicated otherwise in a credit line to the material. If material is not included in the article's Creative Commons license and your intended use is not permitted by statutory regulation or exceeds the permitted use, you will need to obtain permission directly from the copyright holder. To view a copy of this license, visit <http://creativecommons.org/licenses/by/4.0/>.

© The Author(s) 2020